Positron annihilation studies of some anomalous features of $NiFe_2O_4$ nanocrystals grown in SiO_2

S. Chakraverty,* Subarna Mitra,† and K. Mandal‡
C.K. Majumdar Laboratory, S.N. Bose National Centre for Basic Sciences, Block JD, Sector III, Salt Lake, Kolkata 700098, India

P. M. G. Nambissan§
Nuclear and Atomic Physics Division, Saha Institute of Nuclear Physics, 1/AF Bidhannagar, Kolkata 700064, India

S. Chattopadhyay
Department of Physics, University College of Science and Technology, Rajabazar Prangan, 92 A.P.C. Road, Kolkata 700009, India
(Received 26 May 2004; revised manuscript received 23 August 2004; published 28 January 2005)

Nanocrystalline $NiFe_2O_4$ particles were synthesized in a SiO_2 matrix and were characterized by x-ray diffraction and TEM observations. Positron lifetimes in these samples were measured. The measured positron lifetimes indicated admixtures of contributions from annihilations within the nanoparticles, at the nanoparticle-SiO_2 interfaces, and from the SiO_2 matrix. The individual contributions were calculated based on the known characteristics of electron-positron annihilation in solids and they were found in remarkable agreement with the known effects expected from grain size reduction and lattice contraction. However, the anomalous rise in positron lifetimes during the reduction of the grain size below 5.6 nm is a deviation from these expected trends and is attributed to the transformation of the inverse spinel structure of the $NiFe_2O_4$ to the normal phase, with the tetrahedral (or *A*) sites being fully occupied by the divalent Ni^{2+} ions and the Fe^{3+} ions transferred to the octahedral (or *B*) sites. The results of Mössbauer spectroscopic studies supported this argument, as the percentage of Fe^{3+} ions occupying the *A* sites drastically reduced to zero when the grain size of the samples decreased to 4.8 nm and below.

DOI: 10.1103/PhysRevB.71.024115 PACS number(s): 78.70.Bj, 75.50.Gg, 61.46.+w, 61.18.Fs

I. INTRODUCTION

The properties of nanocrystalline ferrites have become subjects of intense research in recent years.[1–4] Besides the potential of ferrites as novel materials for applications in a variety of areas like information storage, color imaging, ferrofluids, microwave devices, and communication technology, the anomalous changes in their fundamental properties when reduced to ultrafine grain sizes have attracted great interest.[5,6] The normal spinel ferrite $Mn_{1-x}Zn_xFe_2O_4$, for example, gets inverted when the grain size becomes smaller than 10 nm.[5] When the divalent Zn^{2+} ions in $ZnFe_2O_4$ are gradually replaced by Ni^{2+} ions, it gets inverted on the basis of octahedral site stabilization energy considerations.[7] Hence it will be fruitful to explore the structural characteristics of $NiFe_2O_4$ at nanometer grain dimensions so that these may be correlated to the changes in their electronic and magnetic properties. Positron annihilation spectroscopy, especially based on the measurements of the lifetime of positrons annihilating in the defects in the lattice of materials, will be very useful to understand some of these aspects. One such study has been recently reported on $ZnFe_2O_4$.[8]

II. EXPERIMENT

$NiFe_2O_4$ ferrite nanoparticles in SiO_2 matrix were prepared by the sol-gel method.[9] The weighed amount of nitrate salts $Ni(NO_3)_2 \cdot 6H_2O$ and $Fe(NO_3)_3 \cdot 9H_2O$ were first dissolved in distilled water and stirred with a magnetic stirrer until a clear solution is obtained. This solution was added to tetraethoxy orthosilicate $[Si(OC_2H_5)_4]$ in such a way that, in the final sample, the ratio of the ferrite and SiO_2 becomes 3:7 by weight. The *p*H of the solution was maintained at 2.0 as the isoelectric point of silica is close to that value of *p*H. The mixture was then stirred again and dried slowly to form gel. The gel was heated at different temperatures starting from 973 K to 1273 K for different hours to get samples of different grain sizes, as mentioned in Table I. X-ray diffraction studies of the prepared samples were carried out using a Philips PW 1710 diffractometer to ensure the actual crystalline structure and phase and the average grain sizes were estimated from the broadening of the peaks using the standard Scherrer formula.[10] The particle size was also estimated from the transmission electron micrographs taken using a JEM-200-CX TEM and the results agreed with those ob-

TABLE I. The temperature and duration of heat treatment used for growing $NiFe_2O_4$ nanoparticles of different sizes (as obtained from XRD) in the SiO_2 matrix. The lattice parameter obtained for the different samples are also given.

Temperature (K)	Duration of annealing (h)	Grain size (nm)	Lattice constant (Å)
973	2	3.5	8.16
1073	1	4.8	8.19
1173	1	5.6	8.22
1273	2	6.8	8.25
1273	5	15.0	8.26
1273	24	25.0	8.27
1273	98	40.0	8.28

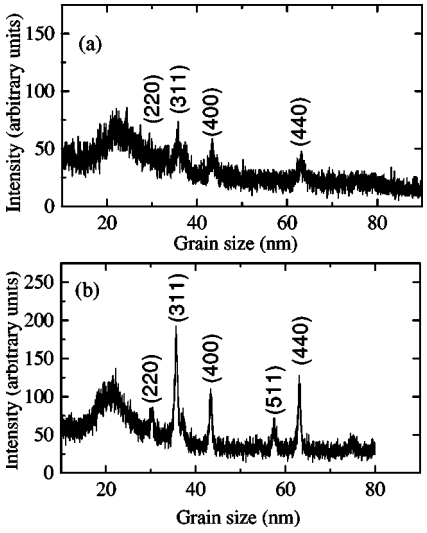

FIG. 1. X-ray diffraction pattern of $NiFe_2O_4$ nanoparticles of average grain size (a) 3.5 nm and (b) 25 nm in SiO_2 matrix.

tained from the XRD data. Further the lattice parameter of the spinel ferrite cubic lattice was also estimated.[11] The average grain sizes and the lattice parameters obtained so are listed in Table I.

Positron annihilation studies were performed by immersing a ^{22}Na source of strength about 400 kBq, deposited and covered by a thin Ni foil, into the powdered sample taken in a glass tube. The glass tube was continuously evacuated during the experiments to keep the sample and source in good vacuum and dry conditions. The powder surrounded the source from all sides for sufficient thickness so as to prevent the annihilation of positrons within the glass walls. The spectra were recorded using a slow-fast gamma-gamma coincidence spectrometer with prompt time resolution of 240 ps (full width at half maximum) for ^{60}Co gamma rays. About 1.5×10^6 counts were collected under each spectrum and the spectra were analyzed using the computer programs RESOLUTION and POSITRONFIT.[12]

The Mössbauer spectra of the samples have been recorded in transmission geometry using CMTE (Model 250) constant acceleration type drive with a 185 MBq ^{57}Co γ-ray source in Rh matrix. A Xe-filled proportional counter has been used as the detector. The data have been acquired in the MCS mode using a 4K PC-based multichannel analyzer.

III. RESULTS AND DISCUSSION

Figure 1 shows the x-ray diffraction (XRD) patterns of two samples—of average grain size 3.5 nm and of 25 nm. All the XRD peaks of the samples correspond to single-phase spinel ferrite $NiFe_2O_4$. No other phase including α-Fe_2O_3 was observed. From the XRD pattern, it is observed that, for the same duration of heat treatment, the peaks become sharper with the increase of temperature. The same effect is also observed if the duration of heat treatment is increased keeping the temperature constant. These indicate the growth of grains and, as mentioned in Table I, the average grain size in the different samples varied from 3.5 nm to 40.0 nm.

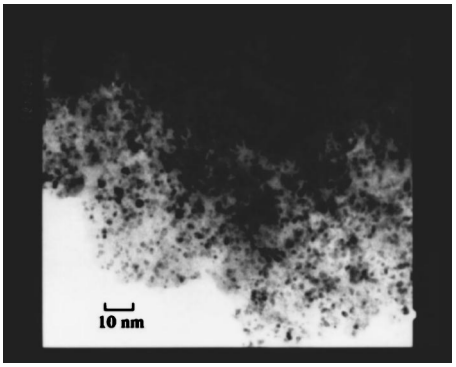

FIG. 2. Transmission electron micrograph of the sample of average grain size 6.8 nm. The magnification is 100 000.

Figure 2 shows a typical TEM micrograph, of the sample prepared by heating at 1273 K for 6 h in this case. The particle size distributions have been found to follow a log-normal distribution[11] and an average grain size of 6.8 nm was estimated for this particular sample. Likewise, the grain size of the other samples were also determined.

The positron lifetime spectra of the SiO_2 sample used as reference in the present work yielded three distinct lifetime components τ_1, τ_2, and τ_3, with relative intensities I_1, I_2, and I_3 (Table II). The longest component $\tau_3=1.62$ ns is due to the annihilation of orthopositronium (*o*-Ps) atoms formed in the pores present in the material. It should be mentioned that the *o*-Ps atoms, with a theoretical lifetime of 140 ns, could be annihilated faster by an electron from the surrounding medium through what is generally known as the pickoff process. In such cases, the resultant lifetime normally do not extend beyond a few nanoseconds. An often used model, proposed by Jean and co-workers,[13] suggests an empirical relation to get the radius of the pore from the measured τ_3 as given below.

TABLE II. Positron lifetimes and their intensities in samples of $NiFe_2O_4$ nanocrystals of different mean grain sizes and grown in SiO_2. The values obtained for the reference SiO_2 are also presented. Typical errors in the lifetimes and intensities are 2 ps, 5 ps, 0.8 ns, 2%, 2%, and 0.1–1.0%, respectively.

Grain size (nm)	τ_1 (ps)	τ_2 (ps)	τ_3 (ns)	I_1 (%)	I_2 (%)	I_3 (%)
3.5	142	432	1.29	52.0	45.1	2.9
4.8	133	406	1.08	50.6	45.2	4.2
5.6	131	392	1.13	50.8	46.2	3.0
6.8	143	420	1.43	56.1	41.7	2.2
15.0	139	416	1.50	54.0	43.3	2.7
25.0	137	400	1.76	55.8	38.5	5.7
40.0	133	400	1.64	51.5	38.9	9.6
SiO_2	116	370	1.62	50.1	27.2	22.7

$$\tau_3 = 0.5\left[1 - \frac{R}{R_0} + \frac{1}{2\pi}\sin\left(\frac{2\pi R}{R_0}\right)\right]^{-1}, \quad (1)$$

where τ_3 is expressed in ns and the radius R in Å. Also $R_0 = R + \Delta R$ where ΔR is the empirical electron layer thickness set equal to 1.66 Å. This results in a pore radius $R = 2.1$ Å. Interestingly, as high as $I_3 = 22.7\%$ of the total events collected under the spectrum resulted from the annihilation of *o*-Ps atoms within the pores (Table II). A pore fraction f_p then can be calculated as

$$f_p = \frac{4}{3}\pi R^3 C I_3, \quad (2)$$

where I_3 is in % and C is 0.0018.[13] This gives a pore fraction of 1.59%. However, a more recent model proposed by Dutta *et al.*[14] had given a more simplified relation as

$$\tau_3 = 1.88R - 5.07 \quad (3)$$

and it gives $R = 3.5$ Å. This may be a slight overestimation as the above relation strictly holds good for *o*-Ps lifetimes above 3 ns only.[14]

Positrons can annihilate from the pores without forming positronium too. The intermediate lifetime τ_2 in fact results from this process. Dannefaer *et al.*[15] had attributed a positron lifetime 300 ps to neutral Si monovacancies or O_2 divacancies in SiO_2. The value of $\tau_2 = 370$ ps which we obtained in our sample is larger than this value and hence it is assigned to the annihilation events from the large number of pores present in it.

The shortest lifetime $\tau_1 = 116$ ps in our sample is once again much smaller than what has been reported ($\tau_1 = 155$ ps) by Dannefaer *et al.*[15] for crystalline SiO_2. As expected, the positronium component there had been a mere 1.5% which might not have significantly affected the value of τ_1. For the presence of a high value of I_3 as in the present case would imply that one-third this intensity out of the actual I_1 would be due to parapositronium (*p*-Ps) formation. This is because when positronium formation takes place, the spin singlet (*p*-Ps) and the spin triplet (*o*-Ps) states are relatively populated by a ratio 1:3. The *p*-Ps lifetime ($\tau_p \sim 125$ ps) then gets admixed with the component of closely lying lifetimes to give τ_1. Hence the contribution to τ_1 from sources other than the *p*-Ps part is estimated as

$$\tau_a = \frac{\tau_1 I_1 - \tau_p I_p}{I_a}. \quad (4)$$

Here I_p as already mentioned is $I_3/3$ and $I_a = I_1 - I_p$. The value of $\tau_a = 114$ ps obtained from the above equation includes the lifetime of positrons annihilating in the defect-free part of the bulk SiO_2 matrix as well as the reduction caused by the Bloch state residence time due to the trapping of positrons in the defects. We consider the positrons forming the *p*-Ps and *o*-Ps atoms as well as those annihilating with the lifetime τ_2 to be in the trapped state and a "mean lifetime" τ_t is defined as

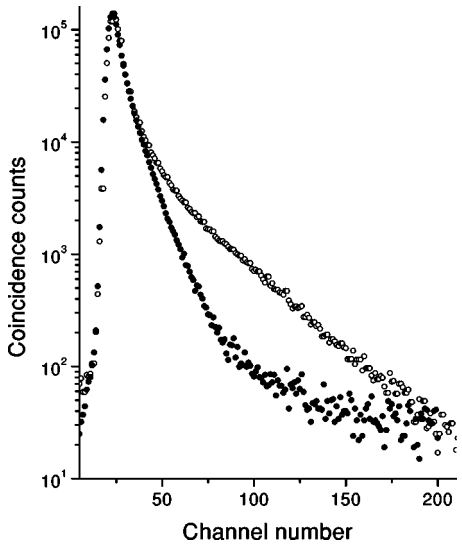

FIG. 3. Peak-normalized positron lifetime spectra of the pure SiO_2 sample (open circles) and the one containing $NiFe_2O_4$ nanoparticles of average grain size 3.5 nm (closed circles).

$$\tau_t = \frac{\tau_p I_p + \tau_2 I_2 + \tau_3 I_3}{I_p + I_2 + I_3}. \quad (5)$$

This is then used in accordance with the two-state trapping model[16] to obtain the lifetime in defect-free region of the SiO_2 matrix. Thus we have used the relation

$$\tau_b = \frac{\tau_a \tau_t}{\tau_a(I_p + I_2 + I_3) + \tau_t(I_1 - I_p)} \quad (6)$$

to obtain the positron lifetime in the bulk defect-free SiO_2 matrix, which turned out to be 226 ps. This is slightly less than but not too far from the value of 238 ps reported for α-SiO_2 (Ref. 15) (the sample used here is amorphous), indicating that the above method of analysis carried out is not unrealistic.

In the SiO_2 samples with the nanoparticles grown in it, we get again three lifetimes τ_1, τ_2 and τ_3 with relative intensities I_1, I_2, and I_3 (Table II). However, the picture is more complicated as is evident from Fig. 3 where due to positron annihilation with the nanocrystalline grains, a faster decaying spectrum is seen visibly distinct from that of pure SiO_2. Thus an additional contribution τ_n from positron annihilation in the nanocrystalline grains will also be admixed with the measured τ_1. The modified relation can be expressed as

$$\tau_1 = \frac{\tau_n I_n + \tau_p I_p + \tau_a I_a}{I_n + I_p + I_a}, \quad (7)$$

where I_n is the intensity of τ_n. Also $I_n + I_p + I_a = I_1$. In order to get the unknown fraction of positrons annihilating in the bulk SiO_2 matrix (now in the presence of the nanoparticles), we note that the value of I_3 has fallen from 22.7% in pure SiO_2 to a significantly reduced value of 2.9% in SiO_2 embedded with nanocrystalline grains of average diameter 3.5 nm. Since this is the reduction in the formation of *o*-Ps, which in other words can be attributed to a reduction in large open volume defects such as pores, it is expected that the positron

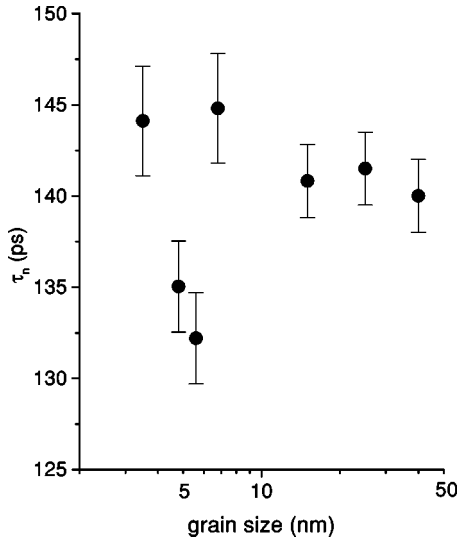

FIG. 4. The derived lifetime τ_n of positrons annihilating within the $NiFe_2O_4$ nanoparticles as a function of the grain size.

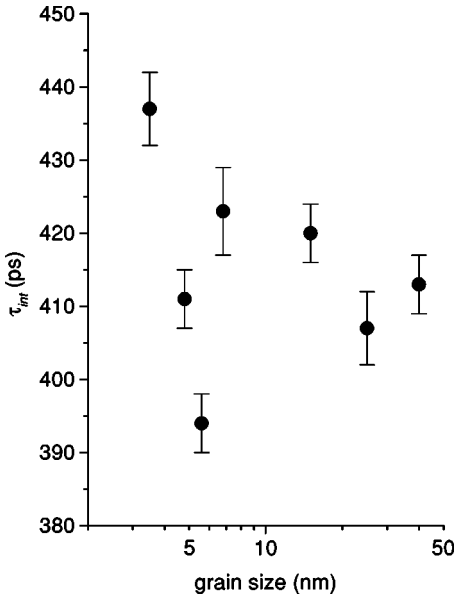

FIG. 5. The derived lifetime τ_{int} of positrons annihilating at the interfaces of $NiFe_2O_4$ nanoparticles and the SiO_2 matrix as a function of the size of the nanoparticles.

annihilation intensity I_2 should also reduce by the same ratio. On the other hand, I_2 is as high as 45.1%, which implies that certain additional trapping sites are also responsible for τ_2 and I_2 in the nanoparticle-embedded samples. These additional trapping sites each can be understood as the pseudogap at the interface of the outermost surface layer of the nanoparticle and the innermost SiO_2 layer surrounding it. This interpretation had been suggested, for example, for the positron trapping at the surfaces of inert gas bubbles in a metal matrix.[17,18] The intensity of that component of the positron lifetime, which comes from the nanoparticle-SiO_2 interface, is estimated as

$$I_{\text{int}} = I_2 - \frac{I_2^s}{I_3^s} I_3, \tag{8}$$

where the superscript denotes the values of I_2 and I_3 for the pure SiO_2 sample, which are 27.2% and 22.7%, respectively. If we assume further that the percentage contribution to I_1 by the intensity of positrons annihilating within the nanoparticles (I_n) is the same as that of I_{int} to I_2, we shall obtain I_n as

$$I_n = \frac{I_{\text{int}}}{I_2} I_1. \tag{9}$$

The intensity of positrons annihilating in the bulk SiO_2 matrix alone then is $I_a = I_1 - I_p - I_n$. These values can then be substituted in Eq. (7) to calculate τ_n, which is the positron lifetime in the nanoparticles. Further, based on all the above assumptions, the lifetime of positrons annihilating at the pseudogap interfaces of the nanoparticles and the SiO_2 is calculated from the relation

$$\tau_2 = \frac{\tau_{\text{int}} I_{\text{int}} + \tau_2^s (I_2 - I_{\text{int}})}{I_2}, \tag{10}$$

where again the superscript implies that $\tau_2^s = 370$ ps. The estimated values of both τ_n and τ_{int} are shown against the grain sizes in Figs. 4 and 5. It should be noted that the positron lifetime at the interface τ_{int} is governed jointly by the electron densities at the surfaces of the nanoparticles and in the SiO_2 matrix. Its value is admixed with the measured τ_2, as seen from an otherwise unexpectedly large value of I_2, as explained above.

The variation of the lifetime parameters τ_n and τ_{int} versus the nanocrystalline grain sizes, as shown in Figs. 4 and 5, depicts three different stages of defect evolution and/or phase transitions. Looking in the direction of decreasing grain sizes from 40 nm to 6.8 nm, the changes in the two lifetimes could be attributed to the expected behavior accompanying the reduction of grain sizes.[19] In an earlier work,[20] it has been shown that the excess free volume associated with the atoms on the grain surfaces increases asymptotically with decreasing grain sizes. Tong *et al.*[21] and Qin *et al.*[22] had also reported that the net defect volume at the nanocrystalline interfaces also increases when the grain size decreases. It may be probably argued that the same is the reason for the sharper rise below 5.6 nm but, as explained later, this change needs more attention. The sharp fall between 6.8 nm and 5.6 nm is a result of the abnormal lattice contraction, as shown in Fig. 6. It is interesting that while elemental nanocrystals like Nb and Ti showed an increase in their lattice parameter,[20,23] compounds like the ferrites have shown a contraction of the lattice.[8]

While the contraction of the lattice in the present samples continued, the two lifetime parameters started increasing remarkably again below the grain size 5.6 nm. In order to understand this unexpected trend, we note that a unit cell of $NiFe_2O_4$ consists of eight such molecules and the total volume occupied by them is about 59.5% of the unit cell. As the unit cell also consists of 64 tetrahedral (or *A*) sites and 32 octahedral (or *B*) sites, it turns out that a volume equivalent to at least 26 tetrahedral sites and 13 octahedral sites is unoccupied and may contain lattice vacancies. Even in the

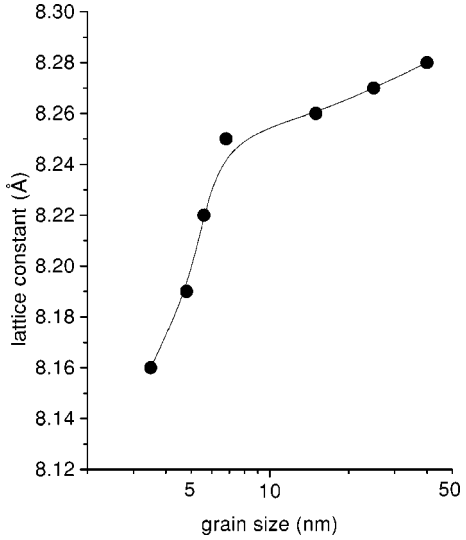

FIG. 6. The lattice parameter (a) estimated from the x-ray diffraction data of the $NiFe_2O_4$ nanoparticles as a function of the grain size.

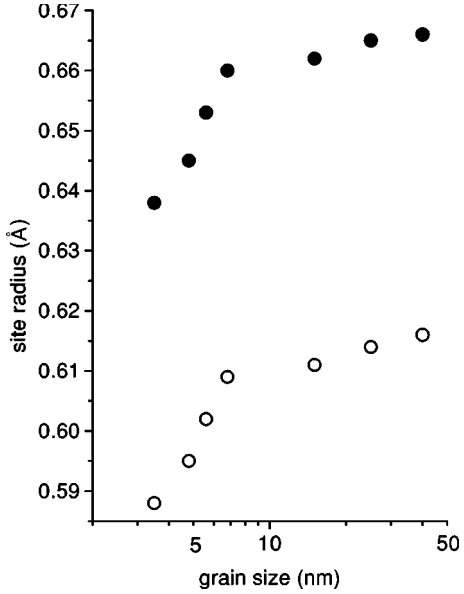

FIG. 7. The radii of the tetrahedral or A sites (open circles) and octahedral or B sites (closed circles) in the $NiFe_2O_4$ nanoparticles as a function of the grain size.

sample of the lowest grain size (3.5 nm) used in the present work, the radii of the A site and B site are 0.59 Å and 0.64 Å, respectively. Although these radii are much less in magnitude than the radius of the monovacancy either in Ni or Fe (~1.24 Å), positrons can be still trapped in them, giving rise to a lifetime less than that in the monovacancies of either Ni [~180 ps (Ref. 24)] or Fe [~170 ps (Ref. 25)]. The values of τ_n that we obtained in the above analysis and showed in Fig. 4 are thus in the expected lines. It should be clarified that the positron thermal diffusion lengths in solids generally are of the order of 50–100 nm,[26] and therefore the thermalized positrons will diffuse out to the surfaces of grains smaller than these lengths before annihilation. Hence we should have expected τ_n to reflect the properties of the grain surfaces. That, however, can be true only in case there are no positron traps within the nanosize grains. In this case however, as already mentioned, the vacant A sites and B sites within the grains would act as saturation traps for positrons, whereas the other derived lifetime parameter τ_{int}, which is the lifetime of positrons directly trapped and annihilated in the grain-SiO_2 interface, can be used to extract information about the structural properties there.

In Fig. 7, the variation of the tetrahedral and octahedral site radius, as calculated from the formula given by Smit and Wijn,[27] with grain size is shown. We note that both the radii decrease when the grain size decreases. The octahedral site radius is, however, larger than the tetrahedral site radius in all the samples. Also, over a wide range of dimensions before it gets a saturation value, the positron lifetime will increase with increase in the size of the vacancy trap.[28] Hence the increase in positron lifetime below the grain size of 5.6 nm as shown in Fig. 4 is possible when there is a change in the predominant positron trapping sites from the tetrahedral sites to the octahedral sites. This can happen, for example, as reported recently in the case of $ZnFe_2O_4$,[8] when an inversion of the spinel structure takes place and the larger size cations fail to occupy the octahedral sites.

We have explored this possibility by carrying out Mössbauer spectroscopy of the samples, which help to determine the relative occupancies of the tetrahedral and octahedral sites by Fe^{3+} ions. Figure 8 gives the Mössbauer specra of some of the samples used in the present work, taken at room temperature. The spectra changes from a two-finger pattern to a six-finger pattern with increase in particle size. The two-finger pattern indicates the superparamagnetic behavior below a particle size of 5 nm. The distribution of cations in the samples has been calculated from Mössbauer subspectral areas. The percentage of Fe^{3+} ions at the A sites is shown in Fig. 9. The bulk $NiFe_2O_4$ in its coarse grained form is a fully

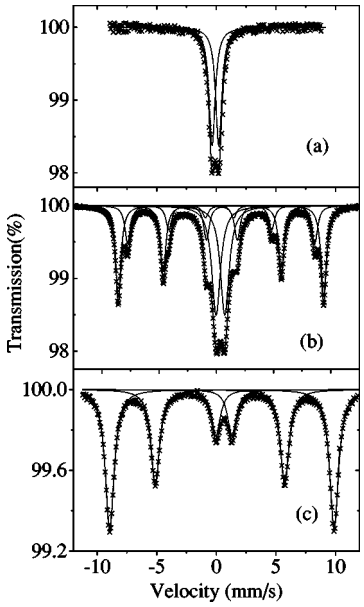

FIG. 8. Mössbauer spectra at room temperature of samples of grain size (a) 3.5 nm, (b) 4.8 nm, and (c) 25 nm.

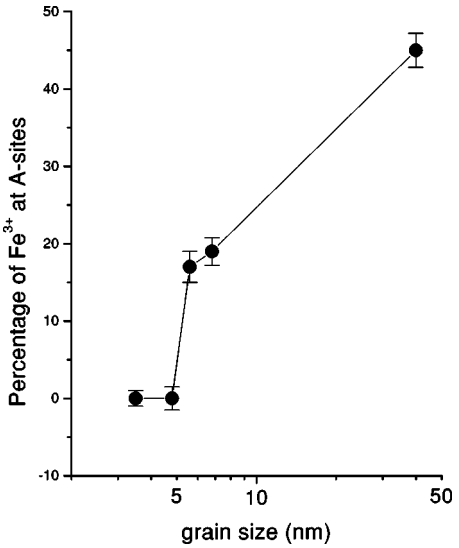

FIG. 9. The percentage of Fe^{3+} ions, as estimated from the Mössbauer spectroscopic data, present at the *A* sites in the $NiFe_2O_4$ nanoparticles as a function of the grain size.

inverted spinel structure with equal number of *A* and *B* sites filled by Fe^{3+} ions.[7] When this structure inverts to the normal spinel configuration, all the Fe^{3+} ions are expected to be at the *B* sites only and the *A* sites are then occupied by the divalent Ni^{2+} ions. Thus, as seen from Fig. 9, the samples of grain sizes 3.5 nm and 4.8 nm are normal spinels and those with grain sizes 5.6 nm and 6.8 nm are mixtures of normal and inverse spinel molecules. During the exchange of the ions between the two sites as a result of this transition, however, not all sites are likely to be filled owing to the extremely low site dimensions brought in by the abnormal lattice contraction.

About the similar rise in the other lifetime parameter τ_{int} at the same region of grain sizes, it may be noted that the atomic reorientation taking place inside the grain may have its bearing on the grain surfaces also. As pointed out by Chen *et al.*[29] in their work on Fe_2O_3 nanoparticles, the surface defects in this class of materials could be the undercoordinated Fe^{3+} sites at the octahedral sites. In the normal spinel ferrites (i.e., those below 5.6 nm in this case), the Fe^{3+} sites are indeed at the octahedral sites and their absence from those sites will leave undersized monovacancies, which would trap positrons.

The behavior of the other positron lifetime parameters with grain size can be explained on the basis of temperature effects rather than those not connected directly with the grains. The steady rise in τ_3 as indicated in Fig. 10 is a result of the temperature treatment carried out in order to have nanoparticles of larger grain sizes. In Table I, already a summary of the temperature and duration of heat treatment carried out to get the samples of the desired mean grain size has been presented. With increase of the temperature, not only the grains grow in size but even the pores will grow in size either by way of agglomeration or with the addition of small vacancy clusters to the pores. Using Eq. (1), we see that the pore sizes varied from 1.7 Å to 2.1 Å. The corresponding intensity component (also shown in Fig. 10) also steadily

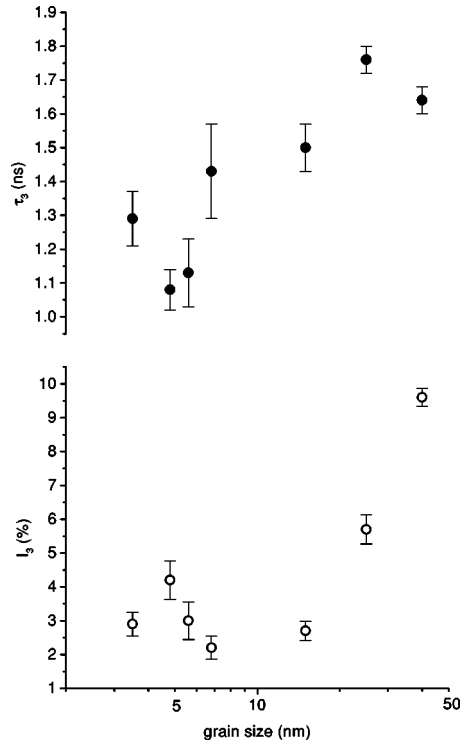

FIG. 10. The orthopositronium lifetime component τ_3 and its intensity I_3 for the $NiFe_2O_4$ (SiO_2) samples as a function of the grain size.

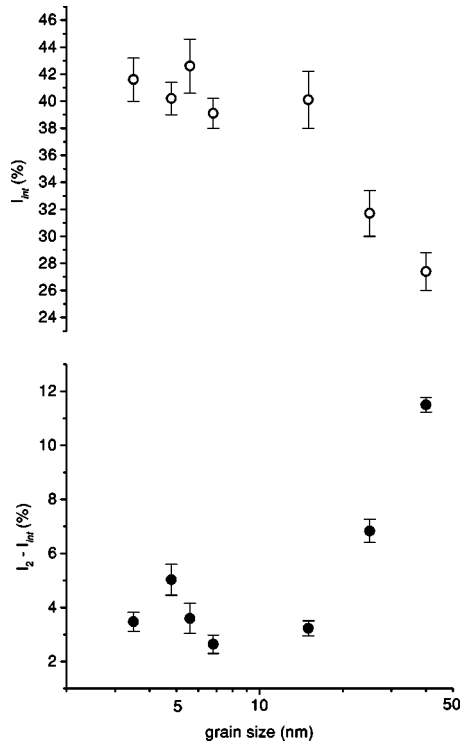

FIG. 11. The interfacial annihilation intensity I_{int} and $I_2 - I_{int}$ for the $NiFe_2O_4$ (SiO_2) samples as a function of the grain size.

increases owing to increased formation of orthopositronium in the SiO_2 matrix. A small abnormal change in the region from 4.8 nm to 6.8 nm however could not be explained.

The other intensity parameter I_2 is split into two parts in accordance with Eq. (8) and the variation of the two parts are shown in Fig. 11. The trends are in the expected lines. The interfacial intensity I_{int} falls down rapidly as the net interfacial area decreases with increasing grain size. The residual intensity will reflect the fraction of positrons annihilating in the pores without forming orthopositronium. Obviously this will follow the behavior similar to that of I_3.

IV. CONCLUSIONS

Certain aspects related to the defects present in nanocrystalline $NiFe_2O_4$ grown in a SiO_2 matrix were investigated through positron lifetime spectroscopy and the study helped in predicting a structural phase transition at very low grain sizes, confirmed by the results of Mössbauer spectroscopy. First, positron lifetime spectra could vividly distinguish between the two systems, i.e., pure SiO_2 and that containing $NiFe_2O_4$ nanoparticles. The resolved positron lifetime parameters further quantified these changes, with a well-defined lifetime component originating from the annihilation of positrons within the nanoparticles. The reduction of the mean grain size to below 6.8 nm affected the tetrahedral and octahedral site radii due to an abnormal lattice contraction. The reduction of the grain size also resulted in transformation of an increasing fraction of the inverted spinel ferrite molecules to the normal spinel structure. This was reflected as a distinct change in the behavior of variation of the positron lifetimes. From Mössbauer spectroscopy, we found that the occupancy of the *A* sites by the Fe^{3+} ions drastically reduced to zero at very low grain sizes, indicating that the material has fully transformed to the normal spinel ferrite structure. The temperature effects on the dimensions of pores in the SiO_2 matrix were also explained as due to an increase in size due to either agglomeration or vacancy-aided growth. We believe that an investigation using the coincidence Doppler broadening spectroscopic method[30] to identify the exact site of annihilation of the positrons will throw further light on these aspects.

ACKNOWLEDGMENTS

The present work was supported by the Department of Science and Technology, Government of India under project Grant No. SP/S2/M-37/2000. Technical help from R. Acharya is also acknowledged.

*Email address: suvankar@bose.res.in
†Email address: subarna@bose.res.in
‡Email address: kalyan@bose.res.in
§Corresponding author. Email address: gopal@anp.saha.ernet.in

[1] T. Sato, K. Haneda, M. Seki, and T. Iijima, Appl. Phys. A: Solids Surf. **50**, 13 (1990).
[2] T. Kamiyama, K. Haneda, T. Sato, S. Ikeda, and H. Asano, Solid State Commun. **81**, 563 (1992).
[3] B. Jeyadevan, K. Tohji, and K. Nakatsuka, J. Appl. Phys. **76**, 6325 (1994).
[4] H. H. Hamdeh, J. C. Ho, S. A. Oliver, R. J. Willey, G. Olivery, and G. Busca, J. Appl. Phys. **81**, 1851 (1997).
[5] C. Upadhyay, H. C. Verma, C. Rath, K. K. Sahu, S. Anand, R. P. Das, and N. C. Mishra, J. Alloys Compd. **326**, 94 (2001).
[6] Sanjukta Ghosh, P. M. G. Nambissan, and R. Bhattacharya, Phys. Lett. A **325**, 301 (2004).
[7] F. Scordari, in *Fundamentals of Crystallography*, edited by C. Giacovazzo (Oxford University Press, New York, 1992), p. 403.
[8] P. M. G. Nambissan, C. Upadhyay, and H. C. Verma, J. Appl. Phys. **93**, 6320 (2003).
[9] K. Mandal, S. Chakraverty, S. Pan Mandal, P. Agudo, M. Pal, and D. Chakravorty, J. Appl. Phys. **92**, 501 (2002).
[10] B. D. Cullity, *Elements of X-ray Diffraction* (Addison-Wesley, Reading, MA, 1978).
[11] K. Mandal, S. Pan Mandal, P. Agudo, and M. Pal, Appl. Surf. Sci. **182**, 388 (2001).
[12] P. Kirkegaard, M. Eldrup, O. E. Mogensen, and N. J. Pedersen, Comput. Phys. Commun. **23**, 307 (1981).
[13] H. Nakanishi, S. J. Wang, and Y. C. Jean, in *Positron Annihilation Studies of Fluids*, edited by S. C. Sharma (World Scientific, Singapore, 1988), p. 292.
[14] Dhanadeep Dutta, Bichitra Nandi Ganguly, Debarshi Gangopadhyay, Tapas Mukherjee, and Binayak Dutta-Roy, J. Phys.: Condens. Matter **14**, 7539 (2002).
[15] S. Dannefaer, T. Bretagnon, and D. Kerr, J. Appl. Phys. **74**, 884 (1993).
[16] D. C. Conners and R. N. West, Phys. Lett. **30**, 24 (1969).
[17] K. O. Jensen and R. M. Nieminen, Phys. Rev. B **35**, 2087 (1987).
[18] K. O. Jensen and R. M. Nieminen, Phys. Rev. B **36**, 8219 (1987).
[19] M. Mukherjee, D. Chakravorty, and P. M. G. Nambissan, Phys. Rev. B **57**, 848 (1998).
[20] P. P. Chattopadhyay, P. M. G. Nambissan, S. K. Pabi, and I. Manna, Phys. Rev. B **63**, 054107 (2001).
[21] H. Y. Tong, B. Z. Ding, J. T. Wang, K. Lu, J. Jiang, and J. Zhu, J. Appl. Phys. **72**, 5124 (1992).
[22] X. Y. Qin, J. S. Zhu, X. Y. Zhou, and X. J. Wu, Phys. Lett. A **193**, 335 (1994).
[23] I. Manna, P. P. Chattopadhyay, P. Nandi, and P. M. G. Nambissan, Phys. Lett. A **328**, 246 (2004).
[24] G. Dlubek, O. Brummer, N. Majendorf, P. Hautojarvi, A. Vehanen, and J. Yli-Kaupilla, J. Phys. F: Met. Phys. **9**, 1961 (1979).
[25] P. Hautojarvi, T. Judin, A. Vehanen, J. Yli-Kaupilla, J. Johansson, J. Verdone, and P. Moser, Solid State Commun. **29**, 855 (1979).
[26] R. M. Nieminen and M. J. Manninen, in *Positrons in Solids*, edited by P. Hautojarvi (Springer-Verlag, Berlin, 1979), p. 145.
[27] J. Smit and H. P. J. Wijn, *Ferrites—Physical Properties of Ferrimagnetic Oxides in Relation to Their Technical Applications* (N.

V. Philip's Gloeilampenfabrieken, Eindhoven, Holland, 1959), Chap. VIII, pp. 136–176.

[28] M. J. Puska and R. M. Nieminen, J. Phys. F: Met. Phys. **13**, 333 (1983).

[29] Lin X. Chen, Tao Liu, Marion C. Thurnauer, Roseann Csencsits, and Tijana Rajh, J. Phys. Chem. B **106**, 8539 (2002).

[30] P. Asoka-Kumar, M. Alatalo, V. J. Ghosh, A. C. Kruseman, B. Nielsen, and K. G. Lynn, Phys. Rev. Lett. **77**, 2097 (1996).